Journal of Electroceramics, 8, 87–98, 2002

Electrostrictive Strain in Low-Permittivity Dielectrics

RATTIKORN YIMNIRUN,[1,*,†] PAUL J. MOSES,[1] ROBERT E. NEWNHAM[1]
& RICHARD J. MEYER, JR[2]

[1]*Materials Research Laboratory, The Pennsylvania State University, University Park, PA 16802, USA*
[2]*Applied Research Laboratory, The Pennsylvania State University, University Park, PA 16804, USA*

Submitted October 5, 2001; Revised March 18, 2002

Abstract. A single-beam interferometer capable of resolving displacements on the order of 10^{-4} Å was used to examine the field-induced displacement in several low-permittivity dielectric materials. The experimental principle and procedures of the single-beam interferometer are described in this article. The importance and the accuracy of the Maxwell stress and the thermal stress corrections are also discussed. We present in this article the field-induced strains and the apparent electrostrictive coefficients of several common dielectric materials, including Al_2O_3, BeO, MgO, AlN ceramics, and SiO_2 glass. Under application of an electric field, these common ceramic materials become thicker in the field direction, while glasses and glass-ceramics get thinner. The magnitude of the displacements varies between 10^{-2} to 10^{-3} Å under 1 MV/m electric field. By comparison, the field-induced displacements in these common electronic materials are approximately 3 to 5 orders of magnitude smaller than those observed in relaxor materials, such as PMN and PVDF, and soft polymers.

Keywords: electrostriction, low-permittivity, dielectrics, interferometer

1. Introduction

Electrostriction is defined as a fourth rank tensor property and the basis of the electromechanical coupling mechanism in all insulators. Magnitudes of electrostrictive effects depend largely upon the type of material. From a practical point of view, electrostrictive stresses can either be seen as a benefit for electromechanical devices, when high strain materials are required, or as a drawback in microelectronics and high voltage devices where the mechanical stresses and strains can lead to breakdowns in insulator materials. Thorough understanding of this fundamental phenomenon is hampered by the lack of experimental data in simple low permittivity dielectrics. This study was undertaken with the primary goal of establishing the reliable and accurate electrostriction coefficients for low permittivity dielectrics.

*To whom all correspondence should be addressed.
†Present address: Department of Physics, Faculty of Science, Chiang Mai University, Chiang Mai 50200, Thailand.

Electrostriction is defined as the quadratic coupling between strain (x) and electric field (E), or between strain and polarization (P). This is a fourth-rank tensor expressed by the following relationships:

$$x_{ij} = M_{ijmn} E_m E_n \tag{1}$$

$$x_{ij} = Q_{ijmn} P_m P_n \tag{2}$$

where x_{ij} is the strain tensor, E_m and E_n are components of the electric field vector, P_m and P_n are components of the polarization vector, and M_{ijmn} and Q_{ijmn} are the fourth rank electrostriction tensors. The M coefficients are defined in units of m^2/V^2. Their values range from about 10^{-24} m^2/V^2 in some low permittivity materials to 10^{-16} m^2/V^2 in high permittivity relaxor ferroelectrics such as lead magnesium niobate-lead titanate (PMN-PT) compositions. Q coefficients are defined in units of m^4/C^2. Q values vary in an opposite way to M values. Q ranges from 10^{-3} m^4/C^2 in relaxor ferroelectrics to greater than 1 m^4/C^2 in low permittivity materials. The polarization-related

electrostriction coefficient Q_{ijmn} is defined to better express the quadratic nature of electrostriction in ferroelectrics and other nonlinear dielectric materials. The M and Q coefficients are equivalent and form the basis of our discussions. Conversion between the two coefficients is carried out using the field-polarization relationships.

Despite the fact that electrostriction was initially relegated to the role of an esoteric, and at best secondary effect, the number of applications of the phenomenon, both theoretical and practical, has been increasing significantly since the introduction of PMN as a prototype electrostrictive material [1]. The development of new materials with large electrostrictive strains results in several applications that take advantage of the electrostrictor as an actuator. The advantages that electrostrictors have over other actuator materials include low hysteresis of the strain-field response, no remnant strain, reduced aging and creep effects, a high response speed, and substantial strains at realizable electric fields [2]. To the other extreme, the interest in the electrostriction exploits its nature as a fundamental property in all insulators. The electrostriction of most low-permittivity dielectrics, such as alkali halide crystals and common ceramics, is very small. The research on these materials is used for a better understanding of the general theory of the elastic and dielectric material properties.

Since electrostriction is present in all insulators, understanding its role in materials is also of practical importance. It has been proposed that electrostrictive stresses may play a significant part in the generation of pressure waves by microwave pulses in dielectrics with thermal or dielectric discontinuities [3]. Electrostrictive self-trapping of light in laser glasses is one of the proposed mechanisms for initiation of laser damage in these glasses [4]. Electrostrictive contribution to the refractive-index intensity dependence in optical fibers due to the change in the material density has been under intensive investigations [5–7]. Though several studies in this area indicate a significant contribution from electrostriction, a definite conclusion cannot be drawn because of the lack of accurate data for the electrostrictive coefficients of silica. Electrostrictive strains arising from high local field concentrations could also initiate fracture in high voltage insulators or in oxide thin films on semiconductors [8–12]. Recently, it has also been proposed that electrostriction is one of the mechanisms responsible for microwave losses in a ferroelectric film [13].

As a fundamental effect, electrostriction may prove to be an important factor in the design of sub-micron electronic devices. The present focus in this area is on synthesis of materials with large electrostrictive effects. The other extreme of the scale may also prove to be of interest. Electrostrictive deformations may be undesirable in devices where fixed geometries are required or components are susceptible to fatigue. As microelectronic devices are taken to smaller dimensions, the increased field levels on the materials can cause quadratic electrostrictive effects ($x \,\alpha\, E^2 \sim 1/t^2$) to predominate over linear piezoelectric effects ($x \,\alpha\, E \sim 1/t$). This effect is illustrated for silica, using the piezoelectric d coefficients of quartz ($d \sim 10^{-12}$ m/V) and electrostrictive M coefficients of silica glass ($M \sim 10^{-22}$ m^2/V^2) in Fig. 1. An applied voltage of 10 V is assumed, and piezo and electrostrictive strains are plotted for devices with increasing thickness. Oxide layers in semiconductors are typically a few nanometers thick. For thicknesses less than 10 nm, which corresponds to the field application of 10 MV/cm or higher, the electrostrictive strain ($\sim$0.1%) can be larger than the piezoelectric contribution, and close to breakdown strains for ceramics and glasses (<0.1%) [14]. Since the breakdown of oxide thin films is found to be about 10 MV/cm [15], it is reasonable to assume that the electrostrictive strain may play a part in the failure mechanisms of ultra-thin films. The argument is still true in other low-permittivity dielectrics, in which even larger electrostrictive strains can be found due to relatively larger M coefficients

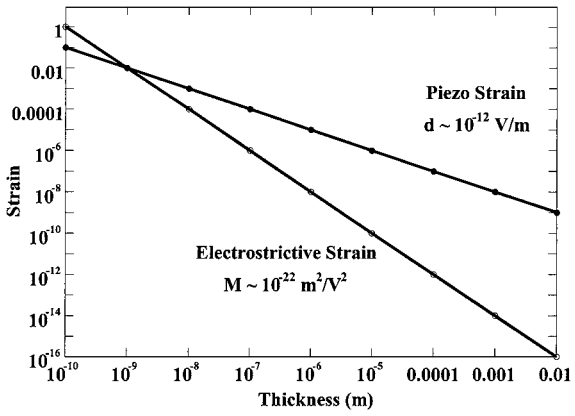

Fig. 1. Strains from piezoelectric quartz and electrostrictive amorphous silica glass plotted for devices of varying thickness with a voltage of 10 V across the device. A typical d coefficient $\sim 10^{-12}$ m/V and an M coefficient of $\sim 10^{-22}$ m^2/V^2 were assumed.

(10^{-21} m^2/V^2). It is then tempting to consider designing a material with zero electrostriction coefficients for applications in areas where field induced damage is a significant risk.

2. Electrostriction Measurements

From the thermodynamic phenomenology of electrostriction, the "direct" effect M and Q electrostriction coefficients are defined as:

$$M_{ijmn} = 1/2\,(d^2 x_{ij}/dE_m dE_n)_x \tag{3}$$

$$Q_{ijmn} = 1/2\,(d^2 x_{ij}/dP_m dP_n)_x \tag{4}$$

Alternatively, by application of the Maxwell relations to the above equations, one can derive the "first converse" effect M and Q coefficients in terms of the dielectric susceptibility (χ_{ij}) and its inverse, the dielectric stiffness tensor (η_{ij}) as:

$$M_{ijmn} = 1/2\,(d\chi_{ij}/dX_{mn})_P \tag{5}$$

$$Q_{ijmn} = -1/2\,(d\eta_{ij}/dX_{mn})_P \tag{6}$$

The "second converse" effect is the polarization dependence of the piezoelectric voltage coefficient (g_{nij}) and can be defined as:

$$M_{ijmn} = \varepsilon_0^2(\varepsilon_{ij} - 1)^2 \delta g_{nij}/\delta P_m \tag{7}$$

$$Q_{ijmn} = \delta g_{nij}/\delta P_m \tag{8}$$

The direct and converse electrostriction effects are of importance because they offer three independent and equivalent techniques for electrostriction measurements: (a) by measuring the strain developed as a function of the field applied, (b) by measuring the change in dielectric susceptibility with applied stress, and (c) by measuring the change in the piezoelectric properties with induced polarization.

Various techniques can be used to determine electrostriction coefficients. Widely used experimental techniques include the strain gauge method, the capacitance dilatometer, and laser ultradilatometer based on Michelson interferometer. Measurements of the direct effect electrostrictive coefficients require the ability to accurately measure very small strains or displacements. Techniques for measuring the converse effect demand precise evaluation of dielectric properties. Generally the electrostrictive displacements vary from sub-angstrom in non-ferroelectrics to sub-micron in ferroelectrics. In ferroelectric ceramics and elastomers, the electrostrictive properties have been extensively studied, but there is very little reliable experimental data for other low-permittivity dielectrics. This arises from measurement difficulties that involve the determination of very small displacements (10^{-1} to 10^{-3} Å in most simple ionic materials, like NaCl, MgO and CaF_2 etc.).

Optical techniques used to detect small electrostrictive strains are advantageous because of their non-contact measurement feature. In addition, they do not need a length calibration and also can be used to profile the sample surface displacements at various locations and under different conditions [16]. A single-beam interferometer is an established instrument that can be used to measure the direct electrostrictive coefficients and has been utilized by many researchers as a tool for measuring the piezoelectric and electrostrictive properties of materials [16–21].

In this article, measurements of the electrostrictive strains in low-permittivity dielectrics, particularly in several common engineering ceramics, with use of the single-beam interferometer are presented. The detailed descriptions of the measurement system are presented elsewhere [22, 23]. However, a brief introduction of the system is presented in the following section.

For monochromatic light with a wavelength λ interfering with a reference beam, the interference intensity at the detector may be expressed as:

$$I = 1/2(I_{\max} + I_{\min}) + 1/2(I_{\max} - I_{\min}) \cos(4\pi\,\Delta d/\lambda) \tag{9}$$

where $I_{\max}$ and $I_{\min}$ are the measured maximum and minimum interference light intensities.

It is desirable to set the interference between the two beams at a point where the light intensity change is maximized for the same Δd change [16]. By differentiating Eq. (9) with respect to Δd, one finds that the maximum change in light intensity occurs when n is an integer and

$$\Delta d = [\lambda(2n + 1)]/8 \tag{10}$$

This setting is called the "$\pi/2$ point" at which the change in optical path is equal to $\lambda/4$. The stabilization system is essentially used to keep the optical path

difference of the interferometer arms constant at $\lambda/4$ by adjusting the electrostrictively driven reference mirror.

For small displacement measurements, we use an A.C. signal detection technique. In such a technique, a small displacement d_{ac} is induced in a sample with an A.C. field. Therefore, near the "$\pi/2$ point" the displacement can be expressed as follows,

$$\Delta d = d_{ac} + [\lambda(2n+1)]/8 \tag{11}$$

For the lowest order ($n = 0$), the variation of the light intensity at the detection point can be re-written as

$$\begin{aligned} I &= 1/2(I_{max} + I_{min}) \\ &\quad -[1/2(I_{max} - I_{min}) \sin(4\pi d_{ac}/\lambda)] \\ &\quad \sim 1/2(I_{max} + I_{min}) \\ &\quad -[1/2(I_{max} - I_{min})(4\pi d_{ac}/\lambda)] \end{aligned} \tag{12}$$

The approximation of $\sin(x) \sim x$ is valid for small x values measured for low permittivity dielectrics, and in this case the error is less than 1% if $|d_{ac}| < 130$ Å [16]. Equation (12) implies that for a small displacement the interference intensity change is linearly proportional to the induced displacement d_{ac}. This makes it possible to determine the field-induced strain in a sample using the A.C. detection technique. For a small sinusoidal displacement,

$$d_{ac} = d_0 \cos \omega t \tag{13}$$

where d_0 is the amplitude of the sample displacement and ω is the frequency of the applied field, Eq. (12) can be expressed as,

$$\begin{aligned} I_{ac} &= 1/2(I_{max} + I_{min}) - [1/2(I_{max} - I_{min}) \\ &\quad \times (4\pi/\lambda)(d_0 \cos \omega t)] \end{aligned} \tag{14}$$

Experimentally, the light intensities (I_{ac}, I_{max}, and I_{min}) are measured with a photodiode, which converts photocurrent to a corresponding voltage. The voltage is observed and measured with an oscilloscope. Hence, at a certain gain, the relationship between the photovoltage and the light intensity may be expressed as,

$$V = \text{constant} \cdot I \tag{15}$$

Consequently, Eq. (14) can be written in terms of the measured voltages as follows,

$$\begin{aligned} V_{ac} &= 1/2(V_{max} + V_{min}) - [1/2(V_{max} - V_{min}) \\ &\quad \times (4\pi/\lambda)(d_0 \cos \omega t) \end{aligned} \tag{16}$$

A root-mean-square (r.m.s.) value of the electrical output V_{ac} is detected by a lock-in amplifier (Stanford Research Systems Model 830) as V_{out}. Since the lock-in amplifier will only detect the A.C. component (ω and its harmonics) of the signal, the $(V_{max} + V_{min})$ component does not contribute to the output reading. The lock-in detection scheme provides excellent noise rejection and is the key to an improved sensitivity. Therefore, it can be shown that

$$V_{out} = V_{r.m.s.} = (\sqrt{2}\pi d_0 V_{p\text{-}p})/\lambda \tag{17}$$

where $V_{p\text{-}p}$ is the peak-to-peak voltage value of the interference signal, which is equal to $(V_{max} - V_{min})$ and corresponds to the change in the interference signal $(I_{max} - I_{min})$. The sample displacement (d_0) may now be expressed as

$$d_0 = (\lambda V_{out})/(\sqrt{2}\pi V_{p\text{-}p}) \tag{18}$$

A single beam interferometer constructed in this study is shown schematically in Fig. 2. The interferometer was modified from the system initially developed by Li et al. [19]. This compact system has a displacement resolution of 10^{-14} m. The total optical path length in the system is small, which is of utmost importance in reducing mechanical noise. The difference in the lengths of the optical path traveled by the two interferometer arms is kept small by mounting the sample, photodiode, and the electrostrictive stack on a small aluminum metal base with an area of 15×15 (cm)^2. The laser is rigidly mounted outside the metal base. All components, except the laser, are placed within an acoustically and thermally isolated box so that the heat generated by the laser does not affect the atmosphere inside the box. This reduces acoustical disturbance and thermal drift, minimizes laser coherence length problems, and compensates for beam divergence. The laser and all components on the metal base are mounted on a compact breadboard (Coherent® Lasertop Breadboard $1' \times 2' \times 2''$). To minimize induced vibrations from the coaxial cables used in the previous system [18], an electrical connection to the sample is achieved through a lead-in "rail". The system is then placed on an industrial-type vibration isolation table to reduce vibrational motions. Temperature, acoustical and electrical stability for the system are achieved by placing the entire system inside an acoustically isolated cabinet.

The laser used is a 2 mW He-Ne laser (Uniphase® Model 1122, $\lambda = 632.8$ nm). The reference mirror,

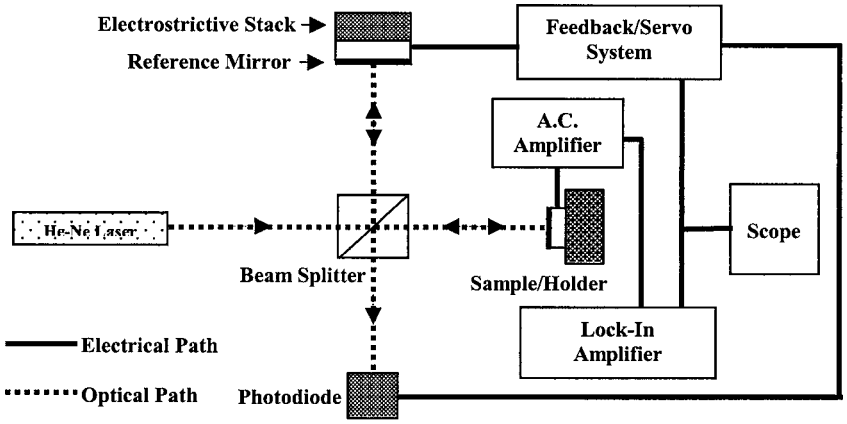

Fig. 2. Schematic of the single-beam interferometer.

which reflects the reference beam, is mounted on an electrostrictive actuator stack connected to a feedback loop. This loop stabilizes the system at a point where the path difference is $\lambda/4$, the so-called "$\pi/2$ point," where the change in light intensity is maximized for a small change in the displacement (Δd) of the sample surface. When an AC field is applied to the sample, small sinusoidal displacements are obtained, giving interference intensity changes at the point of detection. This optical signal is converted to a voltage change by a biased photodiode (Motorola MRD500). The photocurrent is converted to a voltage using a high frequency current to voltage converter with a gain of 10^4 V/A. This voltage is detected by a lock-in amplifier (Stanford Research Systems Model SR830) as V_{out}, an rms value. The interference fringe shifts can be observed using an oscilloscope (Hewlett-Packard 54600B).

3. Corrections for Maxwell and Thermal Stresses

The strain signal observed using the single-beam interferometer is a superposition of true electrostriction and other effects that give rise to a quadratic electromechanical response. In particular, these effects are (a) the electrostatic forces, the so-called the "Maxwell" stress, and (b) the thermal stress. While normally insignificant, these effects must be considered in the measurements of the delicacy and accuracy performed in this study. The Maxwell stress is a result of the attractive forces between the free charges on the electrodes of the sample, which in turn cause a change in dimension in the sample. The thermal stress results from Joule heating that occurs as current flows through the sample. The amount of heating also varies quadratically with the applied field and leads to a corresponding thermal expansion, and additional strain [24, 25]. Therefore, the equation to correct the measured value (M_{ij}^{measured}) for other effects (M_{ij}^{MS} for the Maxwell stress, and M_{ij}^{TS} for the thermal stress) and to obtain the true electrostriction value (M_{ij}) is written as,

$$M_{ij} = M_{ij}^{\text{measured}} - M_{ij}^{\text{MS}} - M_{ij}^{\text{TS}} \tag{19}$$

There have been many different ways to derive the Maxwell stress contribution to electrostriction measurements [24, 26–28]. It is, however, important to emphasize that the correction is dependent on the experimental mechanical boundary conditions of a sample. In a case where the sample is completely clamped, the Maxwell stress correction is expressed as,

$$M_{ijmn}^{\text{MS}} = -(1/2)\, s_{ijmn}\varepsilon_{mn} \tag{20}$$

On the other hand, if the sample is completely free from any mechanical constraints, the correction is written as,

$$M_{ijmn}^{\text{MS}} = -s_{ijmq}\varepsilon_{qn} + (1/2)\,\delta_{pq}s_{ijpq}\varepsilon_{mn} \tag{21}$$

However, in the experimental conditions it is unrealistic to assume that the sample is either completely free from mechanical constraints or completely clamped. It is likely that the sample is in a partially clamped condition. Unfortunately, the exact derivation of the Maxwell stress correction for this condition is still not

available. An approximation can be used to obtain a better correction, but is still open for dispute.

Thermal stress arises from the dielectric losses of the sample under investigation. An exact calculation of the magnitude of the thermal effect is very difficult because of the unknown heat losses involved in the measurements. Under an adiabatic condition, the thermal stress correction M^{TS} for some cubic materials is given by

$$M^{TS} = -(T_0/2C)(\alpha)(\delta\varepsilon/\delta T)_0 \tag{22}$$

where ε is the dielectric permittivity, α the thermal expansion coefficient, C the heat capacity of the sample, T_0 the temperature of a reference state under zero stress and electric field, and T the temperature of the measurement. It has been shown that the thermal stress corrections M^{TS} for many cubic single crystals are on the order of 10^{-23} m^2/V^2 [24]. As a result, the thermal stress correction is usually neglected in most of the electrostriction measurements reported in the past because of its small magnitude in comparison to electrostriction coefficients.

Though the Maxwell stress and the thermal stress corrections are clearly very important in determining the direct electrostrictive coefficients, these corrections are still questionable. It should be emphasized here that more investigations are still needed to correctly determine these corrections. As a result, the measured or apparent coefficients are presented in this article. More importantly, these apparent coefficients are actually more of interest to the engineering community because they directly provide the information on material responses to an applied electric field.

4. Experimental Procedure

Several electrostriction measurements have been reported for alkali halides, alkaline-earth fluorides, and fluoride perovskites. It is, however, very surprising to see that electrostriction coefficients of most common ceramic materials have not been determined, despite their abundant practical applications and availability. It is of interest to measure electrostriction of some of the most common ceramic materials. Many engineering ceramics were examined because of their importance in a variety of circuit boards, electronic components, industrial machines, and ceramic engine parts. Dense polycrystalline specimens of Al_2O_3, A1N, Si_3N_4, Y-ZrO_2, BeO, MgO, TiO_2, several glass-ceramics, and SiO_2 glass (fused quartz or silica) were tested. SiO_2 is of special interest because of its presence in many silicon-based electronic devices and as an integral part of widely used optical fibers.

To exclude effects of the diversity in each engineering material due to different processing techniques, the measurements were carried out on samples obtained from many sources, if possible, and the reported electrostrictive coefficients for each material were averaged from all the samples. The dielectric and structural characterizations of the samples were carried out on an automated LCR meter (HP 4284A Precision LCR Meter), and an x-ray diffractometer, respectively. Other physical information on these materials can also be found in the respective product literature.

The following Al_2O_3 ceramics with different purity (96–99.9%) were obtained from several sources: (1) 99.5% Al_2O_3 (NTK Code: HA-995) from NGK Spark Plugs (U.S.A.), Inc. (NTK) (Santa Clara, California), (2) 99.8% Al_2O_3 from Bolt Technical Ceramics, Inc. (BTC) (Conroe, Texas), (3) MgO-doped Al_2O_3 (99.8%) (SG Code: AF-998) from Saint Gobain/Norton Industrial Ceramic Corp. (SG) (Northboro, Massachusetts), (4) 99.7% Al_2O_3 (Alfa Code: A1-23) from Alfa Aesar (Alfa) (Ward Hill, Massachusetts), (5) 96% Al_2O_3 (Coors Code: AD-96) from Coors Ceramics Company (Coors) (Grand Junction, Colorado), (6) 99.9% Al_2O_3 (Code: AD-999) from National Institute of Standards and Technology (NIST) (Gaithersburg, Maryland), (7) 99.8% Al_2O_3 from the Materials Research Laboratory (MRL) (University Park, Pennsylvania).

AlN ceramics were provided by NTK and Mitsubishi Materials Corporation (Mitsu) (Saitama, Japan). AlN substrate samples provided by Mitsubishi contained approximately 5 wt% of $Y_3Al_5O_{12}$ garnet. Si_3N_4 ceramics were from NTK (NTK Code: EC-141) and SG (SG Code: NBD-200). Yttria-Stabilized ZrO_2 ceramics were from NTK, SG, and Goodfellow Company (GF) (Cambridge, England). Y-ZrO_2 samples from NTK were an ultra-tough partially-stabilized zirconia (NTK Code: UTZ-30), while samples from SG came with two different yttria contents: 2.7 mol% Y_2O_3-ZrO_2 (SG Code: Y-TZP or YZ-110HS), and 3.0 mol% Y_2O_3-ZrO_2 (SG Code: 3Y-TZP). Another yttria-stabilized zirconia purchased from GF was a 3.0 mol% Y_2O_3-ZrO_2 (GF Code: ZR613075). Yttria-Stabilized Zirconia-Toughened Alumina (Y-TZA) ceramic was provided by SG (SG Code: AZ-67HS).

This two-phase ceramic consisted of 20 vol% Y-TZP and 80 vol% Al_2O_3. TiO_2 with 99.6% purity (SG Code: TI603200), and BeO with 99.5% purity (SG Code: BE603100) ceramic samples were purchased from GF. In addition, another high purity BeO ceramic was provided by Dr. Gary L. Messing of MRL, Penn State University. MgO with 98% purity ceramic was purchased from Alfa. This ceramic contains approximately 3–4% porosity with visibly noticeable grain size.

Several types of the fused-SiO_2 glass were used in the measurements. These samples were purchased from GF and Quartz Plus, Inc. (QP) (Brookline, New Hampshire), and were also provided by Saint-Gobain Quartz PLC (Tyne & Wear, England) (SGQ). The sample purchased from GF was a fused-quartz with 99.9% purity (GF Code: SI613140). Many samples from several sources were purchased from the distributing company (QP). These fused-SiO_2 glass samples include: GE 124 semiconductor grade fused quartz, Heraeus Amersil® T08 semiconductor grade fused quartz, NSG OZ semiconductor grade fused quartz, Heraeus Amersil Optosil® fused quartz, Heraeus Amersil Suprasil® synthetic fused silica, Corning® synthetic fused silica, and optical grade fused quartz. The last two samples from SGQ were a transparent and an opaque fused quartz material (Vitreosil®). The purity of all these silica glass samples was more than 99.9%. A borosilicate glass (Schott Code: BOROFLOAT®) and a zero expansion lithia-aluminosilicate glass-ceramic (Schott Code: ROBAX®) were provided by Schott Corporation (Schott) (Yonkers, New York). The primary composition of BOROFLOAT® is as follows: 70–80% SiO_2, 7–13% B_2O_3, 4–8% Na_2O and K_2O, and 2–7% Al_2O_3. ROBAX® is a glass-ceramic consisting of a finely dispersed crystal phase in a glass matrix. The primary glass composition is 50–80% SiO_2, 15–27% Al_2O_3, and 1–5% Li_2O. Corning Incorporated (Corning, New York) also provided another glass-ceramic used in this study. A canasite glass-ceramic (Corning Glass Code: 9634) obtained from Corning consists of about 80% canasite ($K_{3-x}Na_{3-x}Ca_5Si_{12}O_{30}F_4$), where x is equal to or less than unity. This glass-ceramic is a two-phase glass-ceramic material comprised of randomly oriented, interlocking needle-like crystals in a matrix of residual glass. Finally, machinable mica glass-ceramic specimens (NTK Code: TMC-110) provided by NTK were also measured. Mica glass-ceramic has a fairly similar primary composition to that of Corning's Mocor® Machinable Glass Ceramic, which consists of a fluorophlogopite mica phase (55%) interspersed in a borosilicate glass matrix (45%). Additional minor components also exist in the mica glass-ceramic.

Most of the samples were obtained in the form of either thin discs or large square pieces. They were then cut into smaller specimens with an area of approximately 3–5 mm × 3–5 mm and a thickness of 1–2 mm, depending upon sample availability. Samples were carefully polished with plane parallel faces. Residual stress residues from the preparation process were removed by thermal annealing. Gold was sputtered on the sample surfaces to form the top and bottom electrodes. The remaining sides of the samples were then varnished to prevent air breakdown around the samples. For the longitudinal electrostriction measurement, a sample was attached with conductive epoxy adhesive (E-Solder® No 3021 Conductive Adhesives) onto a brass disk 25 mm in diameter and approximately 6–8 mm thick. The brass disk was electrically grounded and served as one electrode for the sample. To provide an optically reflective front surface, a reference mirror made out of a slip cover sputtered with gold, cut to the size of 1.5×1.5 $(mm)^2$, was attached in the middle of the top electrode with the same conductive epoxy. A very fine silver wire (50 μm) was also epoxied to the top electrode away from the laser spot to form a lead-in wire. The lead-in wire was sandwiched between two glass pieces that were glued together with a quickset insulative epoxy. The lead-in wire was bounded carefully to avoid any unwanted motions. Furthermore, the glass-post was also grounded to minimize the attractive force between the lead-in wire and the brass disk, which was believed to cause many unwanted phenomena [22]. The transverse measurements used a slightly different sample configuration that was described previously [23].

Before beginning the experiments, the laser was allowed to stabilize for over an hour to minimize any possible variations. This step was critical because in this technique the sample displacement was determined from variations in laser light intensity caused by the optical path length changes. The experimental steps started by rigidly mounting the brass disk in the sample holder made of a compact and rigid custom optical mount. Electrical connection was then made to the sample through the lead-in "rail". The next critical step was to properly align the laser beam so that the maximum light intensity was achieved at the photodetector. This step was carried out by slightly adjusting both the sample holder and the reference mirror. At this point the interference frings shifts could be observed

on the oscilloscope. The peak-to-peak voltage of the interference pattern was then recorded as $V_{\text{p-p}}$. Then the feedback loop system was used to stabilize the system at a point where the path difference was $\lambda/4$, the "$\pi/2$ point." This maximized the light intensity change for a small change in the displacement of the sample surface.

Samples were then measured by applying an AC field with a superposed DC-bias field. In most cases, the DC-bais was 500 V and the AC field was reduced to 200 V_{rms}. This alleviated the problems observed at higher applied voltages. The magnitude and phase of the output voltage (V_{out}) were recorded from the lock-in amplifier outputs through the computer system. The experiments were done over the frequency range of 3 to 20 kHz. This was the first time that electrostriction measurements on low-permittivity dielectrics were carried out over an extended frequency range. We paid careful attention to the frequency independence of the experimental results because it confirmed the reliability and accuracy of the data. Frequency dependence often indicates the presence of spurious mechanical vibrations or other effects that lead to unreliable measurements. A crucial point was the determination of the sign of the electrostrictive deformation of the sample. Phase information was used to ascertain the sign of the M coefficients. The phase of the pure relaxor PMN was used as a reference since it is known to have a positive M_{11} and a negative M_{12} coefficient.

5. Experimental Results

Measurements were made on more than 14 different ceramics and glasses. We divided these materials into four classes. The first group consisted of three important substrate materials (Al_2O_3, MgO, and BeO). Ceramic materials with higher permittivities ($\varepsilon_r > 10$) Y-ZrO_2, Y-TZA, and TiO_2 made up the second class. Two important nitride ceramics (AlN and Si_3N_4) were in the third class. Finally, SiO_2-glasses and a few glass-ceramics were grouped together in the last class. In the following sections, the results for one representative of each class are presented.

5.1. *Experimental Results on Al_2O_3, MgO, and BeO Ceramics*

Figure 3 shows the field-induced strains obtained from one of the Al_2O_3 ceramic samples when 200 VAC and 500 VDC were applied to the sample. The longitudinal

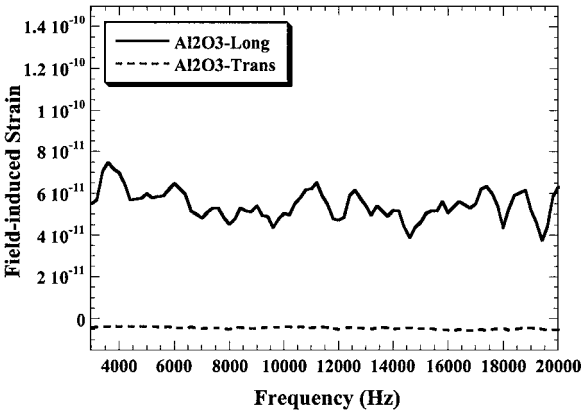

Fig. 3. Field-induced strains as a function of frequency for an Al_2O_3 ceramic (source-MRL) with application of 200 VAC and 500 VDC. The thicknesses in the strain direction are 0.62 and 4.61 mm for the longitudinal and transverse measurements, respectively.

strain was determined to be positive with a magnitude around $+6 \times 10^{-11}$. This corresponds to a displacement on the order of 10^{-14} m. Since the magnitude of the displacement was very small, the result seemed to be scattered. The transverse strain was found to be negative with a much smaller magnitude. MgO and BeO possessed the same signs for the two strains, but with considerably smaller magnitudes. The measured M_{11} and M_{12} coefficients for Al_2O_3 ceramics were determined to be approximately $+0.5$ and -0.05, in units of 10^{-21} m^2/V^2, respectively (Fig. 4). A slight difference in the magnitude of the coefficients was found in MgO and BeO ceramics. Interestingly, the measured M_{11} and M_{12} values of MgO and BeO ceramics were almost equal in magnitude. The values reported for

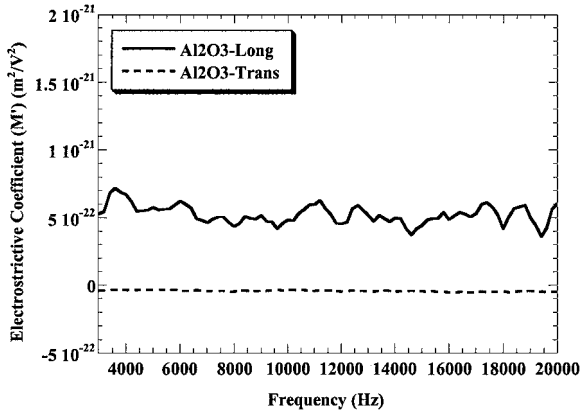

Fig. 4. Measured electrostrictive (M_{11} and M_{12}) coefficients as a function of frequency for Al_2O_3 ceramic (source-MRL).

Table 1. Measured M coefficients of ceramics, glasses, and glass-ceramics.

Material	ε_r	Measured M ($\times 10^{-21}$ m^2/V^2) M_{11}	M_{12}
Ceramics			
Al_2O_3	10.0	+0.47 (±0.12)	−0.13 (±0.04)
MgO	8.1	+0.55 (±0.11)	−0.33 (±0.10)
BeO	6.5	+0.20 (±0.06)	−0.23 (±0.05)
Y-ZrO_2	32.7	+4.51 (±0.68)	+0.33 (±0.07)
TiO_2	92.7	+21.9 (±2.20)	+2.77 (±0.83)
Y-TZA	13.3	+1.05 (±0.21)	−0.14 (±0.03)
AlN	8.5	+0.24 (±0.07)	+0.13 (±0.04)
Si_3N_4	7.9	+0.17 (±0.07)	−0.07 (±0.03)
Glasses and glass-ceramics			
Fused-SiO_2	3.7	−0.18 (±0.07)	−0.18 (±0.07)
Borosilicate glass	4.7	−0.16 (±0.05)	−0.40 (±0.16)
Lithia-aluminosilicate glass-ceramic	8.5	−0.32 (±0.10)	−0.85 (±0.26)
Mica glass-ceramic	5.0	+0.85 (±0.26)	−0.23 (±0.09)
Canasite glass-ceramic	68.0	+3.82 (±0.76)	+1.52 (±0.30)

each ceramic in Table 1 were averaged from measurements on different samples obtained from various sources.

5.2. *Experimental Results on Y-ZrO_2, Y-TZA, and TiO_2 Ceramics*

Since most of the electrostriction measurements have been carried out on high permittivity or very low permittivity dielectrics, it was of interest to examine some dielectrics with moderate permittivity. Y-ZrO_2, Y-TZA, and TiO_2 with dielectric constants (ε_r) of 33, 13, and 93, respectively, were chosen for study. The field-induced strains are plotted as a function of frequency for Y-ZrO_2 in Fig. 5. The longitudinal strain was about two orders of magnitude larger than those observed in other permittivity dielectrics. This strain translated to a displacement of 10^{-13} m. Similar values were observed for TiO_2. However, Y-TZA has a smaller dielectric constant and showed much smaller strains. The transverse strains were measured to be positive in Y-ZrO_2 and TiO_2, and negative in Y-TZA. The measured electrostrictive coefficients are shown in Fig. 6.The measured longitudinal coefficient for Y-ZrO_2 was approximately $+4 \times 10^{-21}$ m^2/V^2, with a much smaller transverse coefficient. The measured electrostrictive

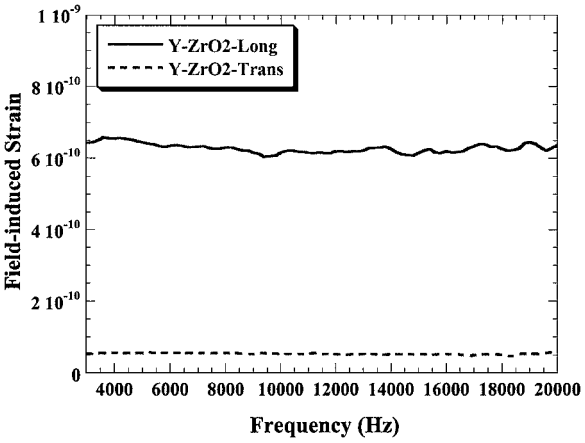

Fig. 5. Measured field-induced strains as a function of frequency for Y-ZrO_2 ceramic (source-Goodfellow) with application of 200 VAC and 500 VDC. The thicknesses in the strain direction were 0.53 and 3.13 mm for the longitudinal and transverse measurements, respectively.

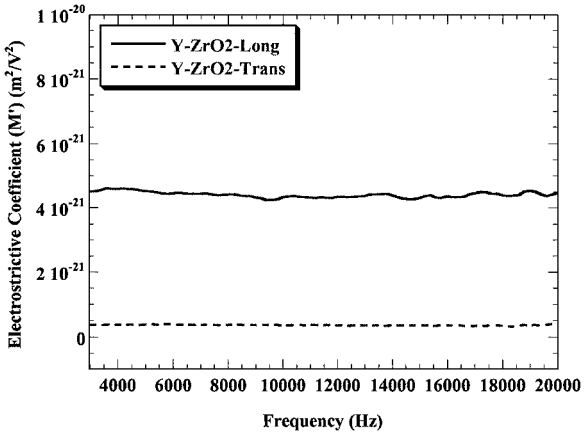

Fig. 6. Measured electrostrictive (M_{11} and M_{12}) coefficients as a function of frequency for Y-ZrO_2 ceramic (source-Goodfellow).

coefficients of TiO_2 were five times as large, which could be attributed to its high dielectric constant. Y-TZA had much smaller coefficients as expected.

5.3. *Experimental Results on AlN and Si_3N_4 Ceramics*

With many potential applications, AlN and Si_3N_4 were the two nitride ceramics selected for the study. Longitudinal and transverse electrostriction measurements were carried out on these two ceramics. Figure 7 shows

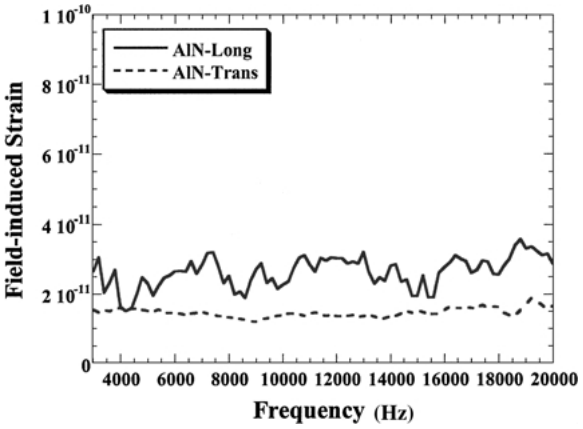

Fig. 7. Measured field-induced strains as a function of frequency for AlN ceramic (source-Mitsubishi).

the frequency dependence of the observed strains for AlN. Both the longitudinal and the transverse strains were found to have a positive sign. The magnitudes were approximately $+2 \times 10^{-11}$, which corresponds to 10^{-14} m in displacement. Even smaller strains were observed on Si_3N_4. The strains measured from both ceramics were close to the limit of the single-beam interferometer. This was the reason why the experimental data appeared to be more dispersive. In contrast to AlN, the longitudinal and transverse strains of Si_3N_4 were determined to have opposite signs. For both ceramics the measured M_{11} coefficients were found to be in the range between $+0.1 \times 10^{-21}$ and $+0.3 \times 10^{-21}$ m^2/V^2, with noticeably smaller values for M_{12} (Fig. 8).

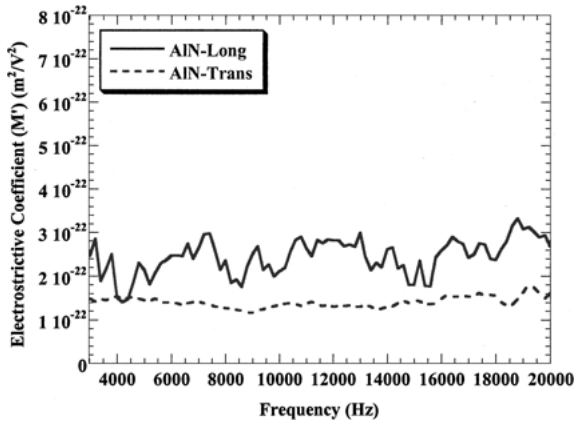

Fig. 8. Measured electrostrictive (M_{11} and M_{12}) coefficients as a function of frequency for AlN ceramic (source-Mitsubishi).

5.4. *Experimental Results on Fused-SiO_2, Glasses, and Glass-Ceramics*

SiO_2 glass is undoubtedly one of the most important materials because of its many optical and electronic applications. SiO_2 films are present in many Si-based electronic components that operate under high electric fields. It was, therefore, very interesting to see how SiO_2 deformed under applied fields. In addition to pure SiO_2, there are many other modified glasses and specialty glass-ceramics that are of interest to our study. Based on availability, the electrostrictive coefficient measurements were performed on the following materials: fused silica, borosilicate glass, lithium-aluminosilicate glass-ceramic, mica glass-ceramic, and canasite glass-ceramic. Figure 9 shows the measured longitudinal and transverse field-induced strains of fused-SiO_2 calculated from the measured displacements. Interestingly, both the longitudinal and transverse strains were negative and very small in magnitude. The magnitude of displacements observed was approaching the instrument limitation. The resulting strains were determined to be on the order of 10^{-12}. Borosilicate glass and lithia-aluminosilicate glass-ceramic exhibited similar strains. It was very interesting to see that the magnitude of the transverse strain in these two materials was noticeably larger than the longitudinal strain. It was also in these two materials that the negative longitudinal and transverse

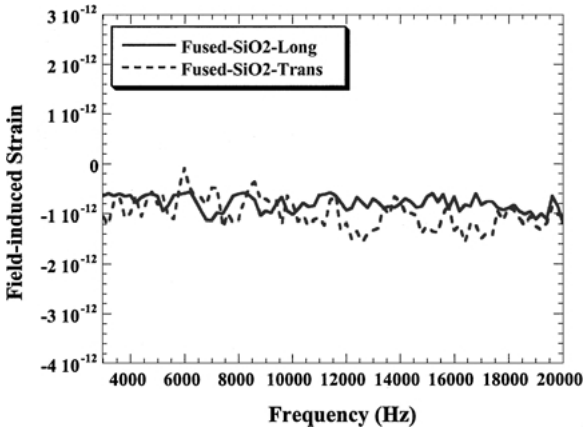

Fig. 9. Measured field-induced strains as a function of frequency for fused silica (source-Goodfellow) with application of 200 VAC and 500 VDC. The thicknesses in the strain direction were 3.10 and 3.74 mm for the longitudinal and transverse measurements, respectively.

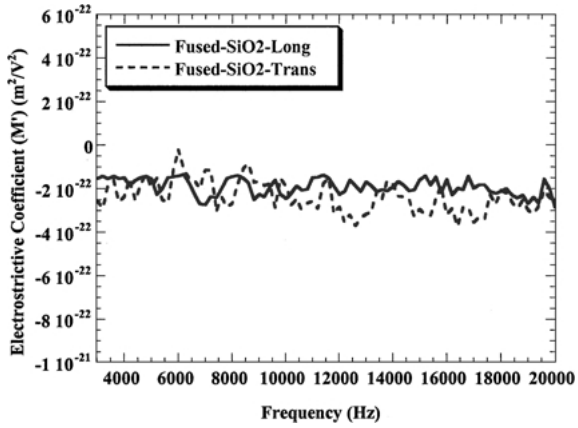

Fig. 10. Measured electrostrictive (M_{11} and M_{12}) coefficients as a function of frequency for fused-SiO_2 (source-Goodfellow).

strains were observed. Canasite glass-ceramic, on the other hand, exhibited positive values for both strains, with much higher magnitude (10^{-11}). This was obviously due to an increased dielectric constant in canasite ($\varepsilon_r \sim 68$). The longitudinal strain in mica glass-ceramic was observed to be positive, while the transverse strain was negative. Its strain magnitude was approximately in the same level as those observed in the low permittivity glasses and glass-ceramics. The measured electrostrictive coefficients were calculated, as shown in Fig. 10, for fused-SiO_2. Except for canasite glass-ceramic, the absolute magnitude of the coefficients fell between $+0.2 \times 10^{-21}$ and $+1 \times 10^{-21}$ m^2/V^2 for all the glasses and glass-ceramics. The measured coefficients of canasite glass-ceramic were approximately $+3.5 \times 10^{-21}$ and $+1.5 \times 10^{-21}$ m^2/V^2 for M_{11} and M_{12}, respectively.

In addition, it should be emphasized that the reported coefficients for Al_2O_3 ceramics and SiO_2 glasses were averaged from the measurements on various samples from several commercial providers. Seven types of Al_2O_3 ceramics with a variation of purity from 96% to 99.9% and ten different types of fused-SiO_2 were measured. In units of 10^{-21} m^2/V^2, the measured M_{11} coefficients of Al_2O_3 ceramics fall between $+0.35$ and $+0.56$, while the measured M_{11} coefficients vary from -0.25 to -0.11 for fused-SiO_2. This suggests that material chemistry may be an important factor in determining the electrostrictive properties in these materials.

6. Comparison with Other Dielectric Materials

To provide a better view of how different types of dielectric materials respond to an applied electric field, we compared the apparent electrostrictive displacement of several materials with the same thickness of 1 mm under an application of 1 kV electric potential (equivalent to 1 MV/m electric field), as shown in Fig. 11. Electrostrictive coefficients of other materials were obtained from literature [2, 23].

Figure 11 clearly demonstrates that under the influence of an electric field materials can either expand or contract depending upon the type of materials. The

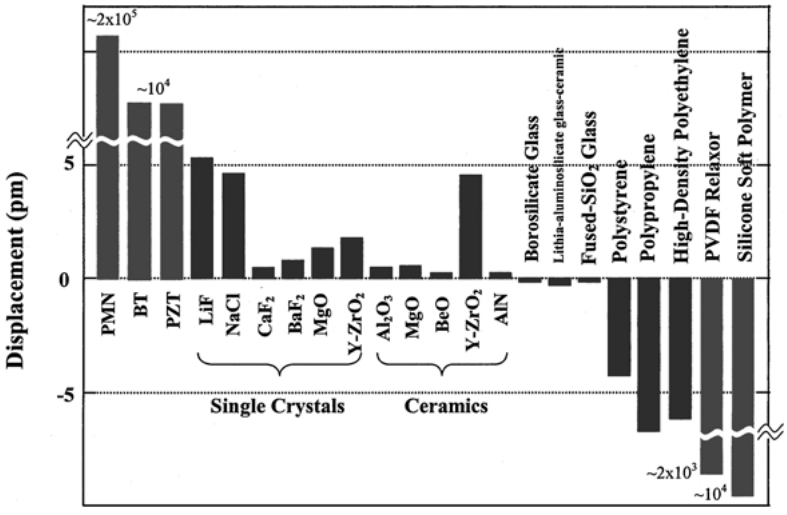

Fig. 11. Comparison of apparent electrostrictive displacements of several types of materials under 1 MV/m electric field application (each sample has the same thickness of 1 mm).

apparent field-induced displacements, which are a combination of contributions from several physical properties including electrostriction and Maxwell stress, range from sub-microns in PMN, PVDF-relaxor, and very soft polymers to sub-angstroms in most common single crystals, ceramics, and glasses. It is also very interesting to observe that glasses, glass-ceramics, and polymers become thinner in the electric field direction, though very much different in magnitudes. On the other hand, most ceramics and single crystals get bigger in the field direction. Both positive and negative values suggest that through mixing rules it is possible to engineer materials that do not change shape under an electric field.

7. Conclusions

Electrostriction is present in all insulators. Most of the previous electrostrictive studies have been undertaken on materials with high electrostrictive strains clearly because of their applications. However with the micro- and nano-electronic revolutions taking place it is interesting to observe that electrostrictive strain and stress are becoming a designing concern in materials with high-field applications. Interestingly, despite their vast applications and abundance, electrostrictive studies in common packaging ceramics were scarce. This was mainly because of the difficulty in measuring extremely small displacement expected in the materials. This study was undertaken to examine the field-induced displacements in several common electronic materials using a single-beam interferometer. The experimental results indicate that the field-induced displacements in common low-permittivity electronic materials are on the order of sub-angstroms. It is also interesting to find that the field-induced displacements can be either positive or negative depending upon the type of materials. Comparison shows that under the same electric field the field-induced displacements in common packaging materials are approximately 3 to 5 orders of magnitude smaller than those observed in PMN and soft polymers.

Acknowledgments

This research is supported in full by the National Science Foundation Grant No. DMR-9634101. The authors thank Jeff Long for his help in construction of this system. Discussions and encouragement generated by Drs. Ahmed Amin, Sedat Alkoy, and Jindong Zhang are greatly appreciated. One of the authors, Rattikorn Yimnirun, would also like to express his sincere appreciation for the financial support from the Royal Thai Government through a scholarship under the Development and Promotion of Science and Technology Talents Project (DPST).

References

1. S.J. Jang, Ph.D. Dissertation, The Pennsylvania State University, University Park, PA (1979).
2. R.E. Newnham, V. Sundar, R. Yimnirun, J. Su, and Q.M. Zhang, *J. Phys. Chem.* B, **101**(48), 10141 (1997).
3. T.C. Guo and W.W. Guo, *IEEE Ann. Report Conf. on Electrical Insulation and Dielectric Phenomena*, **152** (1987).
4. R.M. Waxler, *IEEE J. Quantum Electronics*, **QE-7**(4), 166 (1971).
5. A. Melloni, M. Frasca, A. Garavaglia, A. Tonini, and M. Martinelli, *Opt. Lett.*, **23**(9), 691 (1998).
6. N. Godbout, S. Lacroix, , Y. Quiquempois, G. Martinelli, and P. Bernage, *J. Opt. Soc. Am.* B., **17**(1), 1 (2000).
7. A.C. Liu., M.J. Digonnet, and G.S. Kino, *J. Opt. Soc. Am.* B., **18**(2), 187 (2001).
8. S.M. Sze and G. Gibbons, *Solid State Electronics*, **9**, 831 (1966).
9. S.M. Sze, *J. Appl. Phys.*, **38**, 2951 (1967).
10. E.J. Harari, *Appl. Phys.*, **49**, 2478 (1978).
11. K. Honda, T. Nakanishi, A. Ohsawa, and N. Toyokura, *J. Appl. Phys.*, **62**(5), 1960 (1987).
12. H. Ikezi, Y.R. Lin-Liu, T. Ohkawa, and J.S. deGrassie, *J. Appl. Phys.*, **64**(9), 4717 (1988).
13. O.G. Vendik and A.N. Rogachev, *Tech. Phys. Lett.*, **25**(9), 702 (1999).
14. D.J. Green, *Introduction to Mechanical Properties of Ceramics* (Cambridge University Press, Cambridge, 1998).
15. A.A. Istratov, H. Hieslmair, and E.R. Weber, *Mat. Res. Soc. Bull.*, **25**(6), 33 (2000).
16. Q.M. Zhang, W.Y. Pan, and L.E. Cross, *J. Appl. Phys.*, **63**(8), 2492 (1988).
17. B.J. Luymes, *Rev. Sci. Instrum.*, **54**, 90 (1983).
18. Z.Y. Meng, Th. Kwaaitaal, and W.M.M.M. van den Eijnden, *J. Appl. Phys.*, **21**, 175 (1988).
19. J.-F. Li, P. Moses, and D. Viehland, *Rev. Sci. Instrum.*, **66**(1), 215 (1995).
20. V. Sundar, Ph.D. Dissertation, The Pennsylvania State University, University Park, PA (1996).
21. S. Muensit, E.M. Goldys, and I.L. Guy, *Appl. Phys. Lett.*, **75**(25), 3695 (1999).
22. R. Yimnirun, P.J. Moses, R.J. Meyer, and R.E. Newnham, *Rev. Sci. Instrum.* (2002).
23. R. Yimnirun, Ph.D. Dissertation, The Pennsylvania State University, University Park, PA (2001).
24. G. Kloos, *J. Phys. D: Apple. Phys.*, **28**, 1680 (1995).
25. I. Guy, S. Muensit, and E.M. Goldys, *Appl. Phys. Lett.*, **75**(23), 3641 (1999).
26. J. Grindlay, *Phys. Rev.*, **160**(3), 698 (1967).
27. L. Bohaty and S. Haussuhl, *Acta Cryst.*, A **33**, 114 (1977).
28. H.J. Juretschke, *Am. J. Phys.*, **45**(3), 277 (1977).